Experimental investigations and thermodynamic modelling of the Cr-Nb-Sn-Zr system

P. Lafaye, C. Toffolon-Masclet, J-C. Crivello, J-M. Joubert

Experimental investigations and thermodynamic modelling of the Cr–Nb–Sn–Zr system

Paul Lafaye[a,b], Caroline Toffolon-Masclet [a], Jean-Claude Crivello[b], Jean-Marc Joubert[b*]

[a]DEN-Service de Recherches Métallurgiques Appliquées, CEA, Université Paris-Saclay, F-91191 Gif-sur-Yvette, France

[b]Université Paris Est, ICMPE (UMR 7182), CNRS, UPEC, F- 94320 THIAIS France

[*] corresponding author

Tel.: +33 1 49 78 13 44; Fax: +33 1 49 78 12 03

E-mail address: joubert@icmpe.cnrs.fr

Abstract

This work reports the Calphad modelling of the Cr–Nb–Sn–Zr quaternary system. In a previous paper, the thermodynamic modelling of the Cr–Nb–Sn system has been presented. Since no experimental data were available for the Cr–Sn–Zr ternary system, new experimental data are provided, within this study, on the isothermal section at 900 °C. A ternary *C*14 phase has been identified on the Sn-poor side of the phase diagram. In addition to these experimental data, Density Functional Theory (DFT) calculations are carried out in order to determine formation enthalpies of the stable and metastable phases. At last, the Special Quasirandom Structures (SQS) method is jointly used with DFT calculations in order to estimate the mixing enthalpies of the *A*2 and *A*3 binary solid solutions. Finally, these experimental and calculated data in addition to those from the literature, are used as input data for the Calphad modelling of the Cr–Zr, Nb–Zr and Sn–Zr binary systems and the Cr–Nb–Zr, Cr–Sn–Zr and Nb–Sn–Zr ternary systems. A complete database for the Cr–Nb–Sn–Zr quaternary system is provided.

Keywords: Cr–Nb–Sn–Zr; Calphad; DFT; SQS; thermodynamic databases; assessment; phase equilibrium

1. Introduction

Zirconium alloys are mainly used as fuel cladding and structural materials in Light Water Reactors (LWR) because of their very low thermal neutron absorption coefficient, their excellent mechanical properties and corrosion resistance and the relative stability of their properties under irradiation [1,2]. In order to improve significantly the behaviour of the claddings, both in nominal and accidental conditions, it appears useful to have a better control of the microstructure and phase transformations occurring in these alloys, as a function of temperature and composition. In this frame, a new thermodynamic database dedicated to Zirconium alloys is being developed using the Calphad approach, considering the five following elements Zr, Cr, Fe, Nb, Sn. The novelty of this work relies on the systematic use of the Density Functional Theory (DFT) calculations for the reassessment of the individual binary and ternary subsystems.

This paper presents the Calphad modelling of the Cr–Nb–Sn–Zr quaternary system. In a previous paper [3], we have already presented the thermodynamic modelling of the Cr–Nb–Sn ternary system based on new experimental and calculated data, reassessing the Cr–Nb, Cr–Sn and Nb–Sn binary systems. The Calphad modelling of the Cr-Nb-Sn system is taken from this paper [3], including a new description of the Cr-Sn system. In the present study, a partial isothermal section of the Cr–Sn–Zr system was determined at 1173 K. Note that, to our knowledge, no previous experimental data was available for this ternary system before the present work. This isothermal section exhibits a ternary *C*14 phase on the Sn-poor region. In

addition to the new experimental determination, we provide new DFT calculations of the formation enthalpies of all the quaternary *end-members* of the *C*14, *C*15 and *C*36 phases; of all the *end-members* of the *A*15 phase in the Nb-Sn-Zr system; and of η and $ZrSn_2$ in the Sn-Zr system. DFT calculations on Special Quasirandom Structures (SQS) were performed to determine the mixing enthalpies of the *A*2 and *A*3 binary solid solutions. As it will be discussed in section 4.3.2, a recent publication dedicated to the Calphad modelling of the Sn–Zr system [4] is available in the literature. Unfortunately, Perez *et al.* [4] used the formation enthalpies measured by Meschel *et al.* [5] that exhibit very large deviations from publications [6–8] and from our own DFT calculations. For the Nb–Zr system, a very thorough description is available in the literature [9]. Nevertheless, their authors have rejected some measurements of the monotectoid reaction which appear to be reliable due to a lower oxygen contamination of the samples. Moreover, a recent measurement of the monotectoid reaction temperature [10] shows important gap with the optimized one. At last, a very careful and recent publication dedicated to the Calphad modelling of the Cr–Zr system [11] is available in the literature. Unfortunately, Lu *et al.* [11] used a two-sublattice model for the description of the *C*14 and *C*36 Laves phases that is not compatible with our database.

Thus, the Cr–Zr, Nb–Zr and Sn–Zr binary systems have been reassessed.

The first part of this paper is dedicated to the literature survey of the binary systems; the second part is dedicated to the methodology of our approach and the third part to our results and the Calphad modelling of the different sub-systems of the quaternary system.

2. Literature survey

2.1 The Cr–Zr binary system

2.1.1 Experimental data

The Cr–Zr system has been studied by many researchers [11–24]. This system includes three intermetallic phases, the *C*15, *C*36 and *C*14 Laves phases, ordered at Cr_2Zr stoichiometry. This system presents two eutectic reactions, one eutectoid reaction and two metatectic reactions.

Domagala *et al.* [14], Gebhardt *et al.* [15] and Rumball *et al.* [18] determined the solubility of the terminal solid solutions on the Zr–rich side. In addition, Domagala *et al.* [14] and Svechnikov *et al.* [19] measured the solidus on the Zr-rich side. The liquidus temperatures were measured between the two eutectic reactions by Budberg *et al.* [17] and Petkov *et al.* [20]. In addition, Petkov *et al.* [20], Shen *et al.* [16] and Nemoshkalenko *et al.* [21] determined the homogeneity range of the Laves phases. Petkov *et al.* [20] measured the temperatures of the two metatectic reactions. Moreover, these researchers have reported the existence of the *C*36 phase. A detailed bibliographic review of this system was carried out by Arias *et al.* [22]. More recently, Lu *et al.* [11] conducted new measurements of the Cr solubility in the terminal solid solutions on the Zr-rich side and of the homogeneity range of the *C*15 phase. In addition, Lu *et al.* [11] are the first authors to have published measurements of the Zr solubility in Cr.

2.1.2 Thermodynamic data

Sun *et al.* [23], Chen *et al.* [24], Pavlu *et al.* [12] and Lu *et al.* [11] have calculated the formation enthalpies of the *end-members* of the *C*15 Laves phase. Lu *et al.* [11] have also calculated the formation enthalpies of the *end-members* of the *C*14 and *C*36 Laves phases. In

addition, Lu *et al.* [11] used the SQS method to determine the mixing enthalpy of the *A*2 and *A*3 solid solutions.

2.1.3 Thermodynamic assessment

Many researchers have performed thermodynamic modelling of the Cr–Zr system [25–27]. More recently, Pavlu *et al.* [12] re-evaluated this system according to their own DFT calculations. Finally, Lu *et al.* [11] supplemented the literature with new experimental and calculated data and re-modelled the system.

2.2 The Nb–Zr binary system

2.2.1 Experimental data

The Nb–Zr system exhibits a miscibility gap in the bcc phase and a monotectoid reaction.

The miscibility gap has been measured by Flewitt [28] and Van Effenterre [29]. The durations of the annealing treatments performed by Flewitt [28] were superior to 6500 h. Flewitt [28] has reported a temperature of the monotectoid reaction of 620 ± 10 ° C. This value is in good agreement with those of Rogers *et al.* [30], Knapton [31], Lundin *et al.* [32] and Van Effenterre [29]. On the other hand, the measurements of Dwight [33] and Richter *et al.* [34] report a lower temperature (585 ° C and 590 ° C respectively) probably due to a lower oxygen contamination of the samples. More recently, Kim *et al.* [10] have also reported a temperature of the monotectoid reaction of 585 °C. The solidus and the liquidus were measured by Rogers *et al.* [30] and Lundin *et al.* [32]. The solubility of Nb in α–Zr has been measured by Van Effenterre [29].

2.2.2 Thermodynamic data

To our knowledge, no measurements of thermodynamic data are reported for this system. The mixing enthalpies of the bcc and hcp solid solutions have been calculated by Miedema *et al.* [35] and Colinet *et al.* [36].

2.2.3 Thermodynamic assessment

To our knowledge, the only thermodynamic modelling available for this system is the one of Guillermet in 1991 [9].

2.3 The Sn–Zr binary system

2.3.1 Experimental data

The Sn–Zr system has been experimentally studied by Kwon *et al.* [37] considering the experimental work of Mc Pherson *et al.* [38], Speich *et al.* [39], Gran *et al.* [40], Carpenter *et al.* [41], Arias *et al.* [42] and Perez *et al.* [4].

This phase diagram includes three intermetallic phases: the $ZrSn_2$ phase, the *A*15 phase (Zr_4Sn) and the η phase between the Zr_5Sn_3 and Zr_5Sn_4 compositions.

Mc Pherson *et al.* [38] studied this system between 600 °C and 1500 °C. They have reported the existence of the *A*15 phase but also the Zr_5Sn_3 and $ZrSn_2$ compounds. These authors also measured the solubility in the terminal solid solutions on the Zr-rich side. These measurements were supplemented by those of Speich *et al.* [39], Carpenter *et al.* [41], Arias *et al.* [42] and more recently by Perez *et al.* [4]. Arias *et al.* [42] determined that the *A*15 phase is not stoichiometric but exhibit a small homogeneity range. Kwon *et al.* [37] have shown that the η phase has two different prototypes: Mn_5Si_3 for Zr_5Sn_3 composition and Ti_5Si_4 for Zr_5Sn_4 composition. These two structures are extremely close. Indeed, they have the same space group ($P6_3/mmc$), and only differ from each other by the occupation of site 2*b*: not occupied in the first case, and completely occupied by Sn in the second case. At high temperature, a

homogeneity range has been reported between these compounds [37], corresponding to the partial occupation of site 2*b*. At low temperature, a miscibility gap is observed [4,37]. It should also be noted that the congruent melting temperature of the η phase was established by Kwon *et al.* [37] at 1983 °C. The *A*15 phase is stable at 80 at % Zr, while the stoichiometric composition is 75 at% Zr. This shift on the Zr-rich side is explained by a substitution mechanism. Site 2*a* is occupied by Sn (80 at. %) and Zr (20 at. %) [4].

More recently, Perez *et al.* [4] carried out new measurements of the invariant reactions of this system and measured the miscibility gap of the η phase. They showed the miscibility gap has not a symmetric shape.

2.3.2 Thermodynamic data

The formation enthalpy of the Zr_5Sn_3 compound was measured by calorimetry by Meschel *et al.* [5] at 1473 K. More recently, Baykov *et al.* [6] have reported the DFT calculation of the formation enthalpies of the intermetallic phases of this system. The value calculated by Baykov *et al.* [6] strongly disagrees with the measurements of Meschel *et al.* [5]. Thus, Perez *et al.* [4] performed a homothetic transformation of the DFT calculations of Baykov *et al.* [6] in order to match the experimental value measured by Meschel *et al.* [5]. Very recently, Lumley *et al.* [7] and Liu *et al.* [8] carried out new DFT calculations of the formation enthalpies on the intermetallic compounds of this system. Their calculations were found to be in very good agreement with those of Baykov *et al.* [6].

2.3.3 Thermodynamic assessment

Several thermodynamic evaluations are available for the Sn–Zr system [4,43,44]. The most recent is that of Perez *et al.* [4].

2.4 The Cr–Nb–Zr ternary system

2.4.1 Experimental data

The Cr–Nb–Zr system has been experimentally investigated by Kim *et al.* [45], Kornilov *et al.* [46] and Wang *et al.* [47]. Kim *et al.* [45] and Wang *et al.* [47] have measured the isothermal section at 1100 °C and 1300 °C in the Cr-rich part. Their measurements are in a very good agreement with each other. Kornilov *et al.* [46] determined an isopleth section at 66 at.% Cr. The isothermal section also reveals the existence of a wide two-phase domain *C*15 + bcc.

2.4.2 Thermodynamic data

To our knowledge, there are no experimental or calculated thermodynamic data related to the Cr–Nb–Zr ternary system.

2.4.3 Thermodynamic assessment

The Cr–Nb–Zr system was recently modelled by Lu *et al.* [11]. These researchers have reassessed the Cr–Nb and Cr–Zr systems on the basis of their own DFT and SQS calculations.

2.5 The Nb–Sn–Zr ternary system

2.5.1 Experimental data

The first study devoted to the Nb–Sn–Zr system was carried out by Ivanov *et al.* [48]. They have measured the Sn-poor region of the isothermal section between 500 °C and 1050 °C. Later, Soboleva *et al.* [49] experimentally determined the isothermal section at 950 °C. However, their measurements strongly disagree with those of Ivanov *et al.* [48] and many references are missing. In addition, the isothermal section determined by Soboleva *et al.* [49]

shows an abnormal extension of the bcc solid solution of the Nb–Zr system. Therefore, Korotkova [50] performed new measurements of the isothermal section at 500, 725, 850, 950 and 1050 ° C of the Sn-poor region of this system. The measurements of Korotkova [50] exhibit very good agreements with those of Ivanov *et al.* [48].

This system is characterized by the presence of a miscibility gap in *A*15 phase between Nb_3Sn and Zr_4Sn compositions.

2.5.2 Thermodynamic data and assessment

To our knowledge, there exist neither experimental nor calculated thermodynamic data, nor thermodynamic modelling related to the Nb–Sn–Zr ternary system.

3. Methodology

3.1 Experimental details

The samples were prepared from high purity metals (Cr from Alfa Aesar (99.99%), Sn from Alfa Aesar (99.8%) and Zr "Van Arkel" (55ppm of oxygen) from LTMEX-CEA) by arc melting under argon atmosphere. The alloys were melted five times and turned upside down between each melting. The weight losses were not significant. The samples were then wrapped in molybdenum sheets (less reactive than Ta with the possible presence of liquid Sn) and placed in a silica tube sealed under argon. After annealing, the alloys were quenched by immersion into cold water. Each sample was characterized by XRD at room temperature after crushing it into a fine powder and EPMA after polishing another part of the sample. The diffractograms were measured on a Bruker D8-Advance equipped with a graphite monochromator in the diffracted beam working with the Cu K_α radiation (Bragg-Brentano geometry, 2θ range: 10-120°, step: 0.04°, time per step: 20s). They were analyzed by the Rietveld method to characterize the different present phases (Fullprof program). The EPMA is

a Cameca SX-100. The standards are the pure elements. The analysis of each phase was performed through 30-100 measurements done in different location of the sample surface. The details of samples composition and heat treatment are given in Table 6.

3.2 DFT calculations

The total energies of all the *C*14, *C*15, *C*36, *A*15, η and $ZrSn_2$ structures have been calculated within the framework of the DFT. About the *C*14, *C*15 and *C*36 phases, all ordered compounds have been considered by distributing the four individual atoms on each non-equivalent site. The *C*15 phase is modelled with two-sublattice (SL) yielding the generation of 4^2=16 *end-members*. The *C*14 and *C*36 phases are modelled with three-SL yielding the generation of 4^3=64 *end-members.* The *A*15 is modelled with two-SL in the Nb–Sn–Zr system, yielding to the generation of 3^2=9 *end-members.* The η phase is modelled with 3-SL in the Sn–Zr system (only one having a variable composition) yielding the generation of 2^1=2 *end-members.* All these calculations could be done automatically using the ZenGen code [51] which provides all the necessary DFT input files using the Vienna Ab-Initio Simulation Package (VASP) [52,53].

DFT calculations were done by using the generalized gradient approximation (GGA) with the Perdew-Burke-Ernzerhof (PBE) [54] functional and with projector augmented wave (PAW) pseudo-potentials (PP). The standard potentials of the pure elements were used with 6, 11, 4 and 12 valence electrons for Cr, Nb, Sn and Zr respectively. The calculations are made with a cutoff energy of 600 eV for the plane wave basis set. A dense grid of k-points in the Brillouin zone was used with 16 x 16 x 16 k-points meshing for the *C*15 and *A*15 cubic phases, 16 x 16 x 10 k-points meshing for the *C*14 and *C*36 hexagonal phases, 15 x 15 x 22 k-points meshing for the η phase and 19 x 11 x 11 k-points meshing for the $ZrSn_2$ phase. The relaxation of both lattice parameters and internal atomic position were performed and the convergence is

reached for Hellman-Feynman forces less than 1 meV / Å. After relaxation, the total energies have been finally calculated using the linear tetrahedron method with Blöchl corrections [55]. With respect to the low temperature magnetic state of Cr the calculations are performed with spin polarization.

The formation enthalpy is obtained by subtracting the total energy of the structure calculated by DFT to the molar fraction weighted sum of the energies of the pure elements in their Stable Element Reference (SER, ground-state structures for Cr, Nb, Zr and β−Sn for Sn).

In order to determine the mixing enthalpies of the *A*2 and *A*3 binary solid solution, the SQS method was used [56]. This method consists in generating a series of "special" configurations that reproduces the random disorder of a solid solution at a given composition with a limited number of atoms per unit cell. In the present work, the *A*2 structures have been considered for 0.25, 0.50 and 0.75 binary compositions using 16-atom supercells. Generated structures have been taken from the literature [57,58]. In addition, the 1/16 and 15/16 compositions were also considered to simulate diluted solutions. The mixing enthalpy is calculated by subtracting the total energy of the SQS structure calculated by DFT to the molar fraction weighted sum of the energies of the pure elements in the same structure as the solid solution structure.

3.3 Calphad methodology

The Gibbs energy of each phase is described with respect to the chosen sublattice model within the framework of the Compound Energy Formalism (CEF). For a phase α modelled with two-SL in the A−B−C ternary system, the total molar Gibbs energy is given by:

$$G_m^{\alpha} = {}^{ref}G_m^{\alpha} + {}^{id}G_m^{\alpha} + {}^{ex}G_m^{\alpha}$$

where ${}^{ref}G_m^{\alpha}$ is the Gibbs energy surface of reference and represents the site occupancy weighted average molar Gibbs energy of the ordered structure. ${}^{ref}G_m^{\alpha}$ is defined by:

$$^{ref}G_m^{\alpha} = y_A^{(1)}y_A^{(2)}G_{A:A} + y_A^{(1)}y_B^{(2)}G_{A:B} + y_A^{(1)}y_C^{(2)}G_{A:C} + y_B^{(1)}y_A^{(2)}G_{B:A} + y_B^{(1)}y_B^{(2)}G_{B:B} + y_B^{(1)}y_C^{(2)}G_{B:C} + y_C^{(1)}y_A^{(2)}G_{C:A} + y_C^{(1)}y_B^{(2)}G_{C:B} + y_C^{(1)}y_C^{(2)}G_{C:C}$$

With $G_{i:j} = H_{i:j}^{SER,\alpha} - T * S_{i:j}$; $y_j^{(s)}$ the site occupancy of species *j* on sublattice *s* and $H_{i,j}^{SER,\alpha}$ is the formation enthalpy at 0 K, $S_{i:j}$ is the formation entropy of the ordered configuration defined by the element *i* in the sublattice 1, the element *j* in the sublattice 2.

$^{id}G_m^{\alpha}$ is the molar Gibbs energy of an ideal mixing, based on the number of possible arrangements of the constituents of the phase:

$$^{id}G_m^{\alpha} = RT\sum_{s=1}^{s=2} a_s \sum_i y_i^{(s)} \ln(y_i^{(s)})$$

R is the gas constant and $a_s$the multiplicity of the sublattice s.

The excess Gibbs energy is:

$$^{E}G_m^{\alpha} = y_A^{(1)}y_B^{(1)}y_C^{(2)}L_{A,B:C}^{\alpha} + y_A^{(1)}y_B^{(2)}y_C^{(2)}L_{A:B,C}^{\alpha} + y_A^{(1)}y_B^{(2)}y_C^{(1)}L_{A,C:B}^{\alpha} + y_A^{(2)}y_B^{(1)}y_C^{(1)}L_{B,C:A}^{\alpha} + y_A^{(2)}y_B^{(1)}y_C^{(2)}L_{B:A,C}^{\alpha} + y_A^{(2)}y_B^{(2)}y_C^{(1)}L_{C:A,B}^{\alpha}$$

where the excess parameters $L_{i,j:k}^{\alpha}$ can be expressed as a Redlich-Kister polynomial.

Table 1 summarizes all the calculated phases, their crystallographic description and the selected sublattice model.

4. Results and discussion

4.1 The Cr–Zr binary system

4.1.1 DFT results

Fig. 1 shows the 0 K calculated formation enthalpies of the end-members of the *C*14, *C*15 and *C*36 Laves phase as a function of the mole fraction of zirconium, compared to data from literature.

The calculated mixing enthalpies of the *A*2 and *A*3 solid solutions are reported in Fig. 2 and compared with optimized values obtained in this work and from former assessments.

4.1.2 Selection of data

In this study, all the data we mentioned in the presentation of the system were considered. Indeed, these data present good agreements between them and no incompatibility between the different studies has been revealed. In addition, we have considered our own DFT calculations of the formation enthalpies of the *C*14, *C*15 and *C*36 Laves phases as well as the calculations of the mixing enthalpies of the *A*2 and *A*3 solid solutions.

4.1.3 Calphad assessment

The starting values of the formation enthalpies of the Laves phases as well as the interaction parameters of the solid solutions were taken from our own DFT calculations.

First, we optimized the interaction parameters of the liquid phase. Regular, sub-regular and sub-sub-regular binary interaction parameters (order 2) were used with temperature dependence for each of these parameters.

The formation enthalpies and formation entropies of the stable *end-members* of the *C*14, *C*15 and *C*36 phases (Cr_2Zr stoichiometry) were then optimized according to the literature data and giving a greater weight to our own calculations. On the other hand, the formation enthalpies of the metastable *end-members* were kept fixed to the values computed by DFT during the optimization procedure. In addition, no entropic term was used for the metastable *end-members*.

The homogeneity range of the *C*15 phase was described using regular and sub-regular interaction parameters without temperature dependence. The homogeneity range of the *C*14 phase has been described using regular and sub-regular interaction parameters. On the other

hand, the homogeneity range of the *C*36 phase was described without using any parameter. Fig. 3 shows a good description of the experimental data points obtained by our set of parameters. The optimized parameters are given in Table 2.

4.1.4 Discussion

Our thermodynamic description of the Cr–Zr system was carried out using similar parameters as the one of Lu *et al.* [11]. In addition, the phase diagram shown in Fig. 3 exhibits good agreement with the experimental data. Note that the description of Lu *et al.* [11] differs from ours only in the regions that have not been measured such as the solidus between 1400 °C and 1800 °C on the Cr-rich side. The optimized *ground-state* is in good agreement with our calculations and those of Sun *et al.* [23], Chen *et al.* [24], Pavlu *et al.* [12] and Lu *et al.* [11] as shown in Fig. 1. Moreover, the mixing enthalpies we have optimized present a good agreement with our calculations as well as those of Lu *et al.* [11] as reported in Fig. 2. Finally, note that our description uses a three-SL model for the *C*14 and *C*36 Laves phases in contrast to the one of Lu *et al.* [11].

4.2 The Nb–Zr binary system

4.2.1 DFT results

The calculated mixing enthalpy of the *A*2 and *A*3 solid solutions are reported in Fig. 4 and compared with optimized enthalpies obtained in this framework and with data from the literature.

4.2.2 Selection of data

All the experimental and calculated data we mentioned in the presentation of the system were considered. In addition, we have taken into account our own DFT calculations of the mixing

enthalpies of the *A*2 and *A*3 solid solutions. Just note that a greater weight has been assigned to the data of Dwight [33] and Richter *et al.* [34] compared to the other measurements of the monotectoid temperature due to the probable lower oxygen contaminations of the samples.

4.2.3 Calphad assessment

The starting values of all the parameters (except for the interaction parameters of the *A*2 solid solution) were taken from the former assessment of Guillermet [9].

We have optimized the interaction parameters of the *A*2 and *A*3 solid solutions according to our DFT calculations and the data from the literature. For this purpose, regular and sub-regular binary interaction parameters with temperature dependence for the regular parameter were used for the *A*2 solid solution and a regular binary interaction parameter without temperature dependence was used for the *A*3 solution solid. The interaction parameters of the liquid phase were optimized according to the data of the literature. We used regular and sub-regular binary interaction parameters without temperature dependence. The formation enthalpies of the metastable *end-members* of the Laves phases were fixed to the values calculated by DFT. In addition, no entropic term was used for the metastable *end-members*.

Fig. 5 shows a good agreement between the calculated data and the experimental data points. The optimized parameters are given in Table 3.

4.2.4 Discussion

Our thermodynamic description of the Nb–Zr system has been done using one more parameter than the one of Guillermet [9]. Nevertheless, our description shows slightly better agreements with the experimental determination of the monotectoid temperature and the miscibility gap in the *A*2 phase than the one of Guillermet [9] as shown in Fig 5. Moreover,

our thermodynamic assessment is in better agreement with our calculations of the mixing enthalpy of the *A*3 solid solution than the one of Guillermet [9] as reported in Fig 4.

4.3 The Sn–Zr binary system

4.3.1 DFT results

Fig. 6 shows the 0 K calculated formation enthalpies of the end-members of the *A*15, η and the stoichiometric $ZrSn_2$ compound as a function of the mole fraction of zirconium, compared to data from literature.

The calculated mixing enthalpies of the *A*2 and *A*3 solid solutions are reported in Fig. 7 and compared with optimized values obtained in this work and from former assessments.

4.3.2 Selection of data

In this work, we have rejected the formation enthalpy measured by Meschel *et al.* [5] as well as the mixing enthalpy of the liquid phase reported by Valishev [59] and Sudavtsova [60]. Indeed, the values of Meschel *et al.* [5] were not considered because of the very strong disagreement with all the calculated values available in the literature and our own calculations. Further, since no EPMA measurements were made after the reaction, it is possible that the reaction was not complete or that a reaction occurred with the crucible.

The mixing enthalpy reported by Valishev [59] and Sudavtsova [60] were rejected because these measurements strongly disagrees with each other.

4.3.3 Calphad assessment

The formation enthalpies of the *A*15 and η phases as well as the binary interaction parameters of the *A*2 and *A*3 solid solutions were fixed to the values computed by DFT.

We optimized the interaction parameters of the liquid phase. For this purpose, regular and sub-regular binary interaction parameters were used with temperature dependence for the regular parameter. The formation enthalpy and entropy of $ZrSn_2$, η and the stable *end-member* of the *A*15 phase were optimized according to the literature data and giving a greater weight to our own calculations. On the other hand, the formation enthalpies of the metastable *end-members* of the *C*14, *C*15, *C*36 and *A*15 phase were kept fixed during the optimization procedure. In addition, no entropic term was used for the metastable *end-members*. The homogeneity range and the miscibility gap of the η phase have been optimized according to the experimental data reported by Perez *et al.* [4] and Mc Pherson *et al.* [38]. Regular and sub-regular interaction parameters with temperature dependence were used. The *A*2 solid solution was described using regular and sub-regular interaction parameters with temperature dependence. The *A*3 solid solution has required the use of a regular, sub-regular and sub-sub-regular interaction parameter with temperature dependence for the regular and sub-regular interaction parameters.

Fig. 8 shows a good description of the experimental data points obtained by our set of parameters. The optimized parameters are given in Table 4.

4.3.4 Discussion

Our thermodynamic description of the Sn–Zr system has been done using comparable parameters as the one of Perez *et al.* [4].

The calculated phase diagram reported in Fig. 8 presents a slightly better agreement with the experimental data points than the one modelled by Perez *et al.* [4] particularly for the homogeneity range of the *A*15 phase. Moreover, the optimized *ground-state* exhibit an excellent agreement with both the DFT calculations available in the literature and our own as shown in Fig. 6 contrary to the description of Perez *et al.* [4]. Similarly, the mixing enthalpies

we have optimized present a much better agreement with our DFT calculations than those reported by Perez *et al.* [4], as shown in Fig. 7

4.4 The Cr–Nb–Zr ternary system

4.4.1 Calphad assessment

We have re-evaluated the Cr-Nb-Sn system only using two ternary interaction parameters. Note that the description of the *A*2 solid solution was taken from Lu *et al.* [11].

4.4.1 Results

The calculated isothermal section at 1300 °C of the Cr–Nb–Zr system is reported in Fig. 9.

4.4.3 Discussion

The thermodynamic modelling reported by Lu *et al.* [11] is in very good agreement with the various experimental studies. However, the choice of parameters used by Lu *et al.* [11] has to be discussed. Indeed, in order to describe the original shape of the *C*15 phase in the isothermal section at 1100 °C [45], Lu *et al.* [11] used two binary interaction parameters for the *C*15 phase in the Nb–Zr system in addition to a ternary parameter. Since the *C*15 phase is not stable in the Nb–Zr system, the physical meaning of interaction parameters between two metastable *end-members* is not obvious and should be avoided. Moreover, the shape of the *C*15 phase is due to the repulsive character of bcc solid solution of the Nb–Zr system but also to the presence of the metastable *C*15-Nb_2Zr compound close to the stability.

The thermodynamic modelling of the Cr–Nb–Zr reported here was carried out using less parameters than Lu *et al.* [11] while presenting a comparable agreement with the experimental data points as represented in Fig. 9.

All the parameters we used and optimized are summarized in Table 5.

4.5 The Cr–Sn–Zr ternary system

4.5.1 Experimental results

Table 6 summarizes the chemical composition, annealing treatment and the structure and composition of the different phases of the Cr–Sn–Zr samples synthesized in the present work.

The calculated isothermal section at 900 °C of the Cr–Sn–Zr system is reported in Fig. 10. It is noteworthy that a ternary *C*14 phase was observed in the investigated equilibria.

4.5.2 Calphad assessment

The formation enthalpies of the ternary *C*14 *end-members* were fixed to the values computed by DFT. We optimized the entropic contribution of the ternary *C*14 *end-member* which composition is closer to that of the ternary *C*14 phase observed in this paper. In addition, a regular interaction parameter was used for the *C*14 phase.

4.5.3 Discussion

The calculated isothermal section reproduces the observed phase equilibria. Calculated compositions match the experimental ones to within ± 1 at.%.

All the parameters we used and optimized are summarized in Table 7.

4.6 The Nb–Sn–Zr ternary system

4.6.2 Calphad assessment

In order to model the Nb–Sn–Zr ternary system, all the phase equilibria reported by Ivanov *et al.* [48] and Korotkova [50] were considered.

The miscibility gap in the *A*15 phase was optimized using three ternary interaction parameters. In addition, we used a ternary interaction parameter to assess the homogeneity range of the *A*2 solid solution.

4.6.1 Results

The calculated isothermal sections at 950 °C and 1000 °C of the Nb–Sn–Zr system are reported in Fig. 11 and Fig. 12.

4.6.3 Discussion

Our thermodynamic modelling of the Nb–Sn–Zr system presents a reasonable agreement with the measurements of Ivanov *et al.* [48] and Korotkova [50] as shown in Fig. 11 and 12. Just note that their samples were only characterized by X-ray diffraction without phase composition measurements. For example, the solubility of Zr in *A*15-Nb_3Sn was not measured, resulting in very different possible interpretation of their data. Our description describes all the reported data.

All the parameters we used and optimized are summarized in Table 8.

5. Conclusions

The thermodynamic modelling of the Cr–Nb–Sn–Zr quaternary system has been performed using the Calphad approach according to our new experimental and calculated data. Note that the thermodynamic modelling of the Cr–Nb–Sn system was presented in a previous paper [3] and the assessment of the Cr-Sn has since been slightly modified.

The experimental study has been carried out in order to determine several phase equilibria in the isothermal section at 900 °C of the Cr–Sn–Zr system, a system for which no experimental data was available. We have reported the existence of a ternary *C*14 phase in the Sn-poor region of the phase diagram.

Besides, the formation enthalpies of all the *end-members* of the *C*14 (3SL), *C*15 (2SL), *C*36 (3SL), *A*15 (2SL), η (1SL) phases and stoichiometric $ZrSn_2$ have been calculated using DFT. The SQS method was applied to provide robust and consistent values of mixing

enthalpies of the *A*2 and *A*3 solid solutions in the complete composition range for each, outside their stability range. This is particularly important for extrapolation into higher order systems since it does not extend in any of the binary systems.

At last, these experimental and calculated data in addition to the data available in the literature were used as input data for the Calphad modelling of the Cr–Zr, Nb–Zr and Sn–Zr binary systems. Note that the reassessment of the Sn–Zr system leads to a significant shift of the *ground-state* of the system. The Cr–Zr system has been reassessed in order to provide consistent description of the Laves phases and the Nb–Zr system has been modelled with a lower temperature of the monotectoid reaction. Ternary interaction parameters were used to model the Cr–Nb–Zr, Cr–Sn–Zr and Nb–Sn–Zr ternary systems. No quaternary parameter is needed and the quaternary database can be constructed by a combination of the systems we have presented.

Fe is planned to be added to the present database. The complete Cr–Fe–Nb–Sn–Zr quinary system will be presented in an upcoming paper.

Acknowledgements

Eric Bouaravong and Didier Hamon are acknowledged for the synthesis and EPMA measurements, respectively.

SQS and DFT calculations were performed using HPC resources from GENCI-CINES (Grant 2017-096175 and den0006).

GdR ThermatHT is acknowledged for the scientific support.

EDF and AREVA are acknowledged for their financial support.

References

[1] C. Lemaignan, A.T. Motta, Zirconium Alloys in Nuclear Applications, in: Mater. Sci. Technol., Wiley-VCH Verlag GmbH & Co. KGaA, 2006.

[2] J.-P. Mardon, Matériaux des tubes de gainage pour réacteurs à eau pressurisée, Techniques de l'ingénieur, bn3700, 2008.
[3] P. Lafaye, C. Toffolon-Masclet, J.-C. Crivello, J.-M. Joubert, Thermodynamic modelling of the Cr-Nb-Sn system, Calphad-Comput. Coupling Phase Diagr. Thermochem. 57 (2017) 37–45.
[4] R.J. Perez, C. Toffolon-Masclet, J.-M. Joubert, B. Sundman, The Zr-Sn binary system: New experimental results and thermodynamic assessment, Calphad-Comput. Coupling Phase Diagr. Thermochem. 32 (2008) 593–601.
[5] S.V. Meschel, O.J. Kleppa, Standard enthalpies of formation of some 3d, 4d and 5d transition-metal stannides by direct synthesis calorimetry, Thermochim. Acta. 314 (1998) 205–212.
[6] V.I. Baykov, R.J. Perez, P.A. Korzhavyi, B. Sundman, B. Johansson, Structural stability of intermetallic phases in the Zr-Sn system, Scr. Mater. 55 (2006) 485–488.
[7] S.C. Lumley, S.T. Murphy, P.A. Burr, R.W. Grimes, P.R. Chard-Tuckey, M.R. Wenman, The stability of alloying additions in Zirconium, J. Nucl. Mater. 437 (2013) 122–129.
[8] S. Liu, Y. Zhan, J. Wu, X. Wei, Insight into structural, mechanical, electronic and thermodynamic properties of intermetallic phases in Zr-Sn system from first-principles calculations, J. Phys. Chem. Solids. 86 (2015) 177–185.
[9] A. Guillermet, Thermodynamic Analysis of the Stable Phases in the Zr-Nb System and Calculation of the Phase-Diagram, Z. Met. 82 (1991) 478–487.
[10] H.-G. Kim, J.-Y. Park, Y.-H. Jeong, Phase boundary of the Zr-rich region in commercial grade Zr–Nb alloys, J. Nucl. Mater. 347 (2005) 140–150.
[11] H.-J. Lu, W.-B. Wang, N. Zou, J.-Y. Shen, X.-G. Lu, Y.-L. He, Thermodynamic modeling of Cr–Nb and Zr–Cr with extension to the ternary Zr–Nb–Cr system, Calphad-Comput. Coupling Phase Diagr. Thermochem. 50 (2015) 134–143.
[12] J. Pavlu, J. Vrest'al, M. Sob, Stability of Laves phases in the Cr-Zr system, Calphad-Comput. Coupling Phase Diagr. Thermochem. 33 (2009) 382–387.
[13] K. Zeng, M. Hamalainen, L. Kaj, Thermodynamic Modeling of the Laves Phases in the Cr-Zr System, Calphad-Comput. Coupling Phase Diagr. Thermochem. 17 (1993) 101–107.
[14] R. Domagala, D. Mcpherson, M. Hansen, System Zirconium-Chromium, Trans AIME. 197 (1953) 279–283.
[15] E. Gebhardt, J. Rexer, G. Petzow, Zirconium-Tantalum-Chromium-System, Z. Met. 58 (1967) 534-541.
[16] Y. Shen, O. Paasche, On Transformation of ZrCr2, Trans. Metall. Soc. Aime. 242 (1968) 2241.
[17] P.B. Budberg, S.P. Alisova, R.S. Musaev, Izv Akad Nauk SSSR Met. 3 (1968) 222.
[18] W. Rumball, F. Elder, Phase Equilibria in Zirconium-Rich Zirconium-Chromium-Oxygen Alloys, J. -Common Met. 19 (1969) 345-358.
[19] V.N. Svechnikov, A.T. Spektor, Izv SSSR. 4 (1971) 201.
[20] V. Petkov, S. Prima, L.A. Tret'yachenko, Y. Kocherzhinskii, Laves Phases in the System Zirconium-Chromium, Metallofiz. Noveishie Tekhnologii. 46 (1973) 80.
[21] V.V. Nemoshkalenko, A.P. Nesenyuk, V.P. Krivitskii, V. Petkov, L.I. Nikolaev, A.V. Polenur, B.P. Memko, A.P. Shpak, M.A. Mindlina, Metallofiz. Noveishie Tekhnologii. 52 (1974) 54.
[22] D. Arias, J.P. Abriata, The Cr-Zr System, in: Bull. Alloy Phase Diagr., Metals Park, Ohio : American Society for Metals, 1986: pp. 237–243.

[23] J. Sun, B. Jiang, Ab initio calculation of the phase stability, mechanical properties and electronic structure of ZrCr2 Laves phase compounds, Philos. Mag. 84 (2004) 3133–3144.
[24] X.-Q. Chen, W. Wolf, R. Podloucky, P. Rogl, Ab initio study of ground-state properties of the Laves phase compounds TiCr2, ZrCr2 and HfCr2, Phys. Rev. B. 71 (2005) 174101.
[25] L. Kaufman, H. Nesor, The Cr-Zr system, Air Force Mater. Lab. Tech. Rep. AFML-TR-73-36. (1973).
[26] L. Kaufman, H. Nesor, Treatise on Solid State Chemistry, Plenum Press, 1975.
[27] T. Chart, F. Putland, Thermodynamically Calculated Phase-Diagram for the Co-Cr-Zr System, Calphad-Comput. Coupling Phase Diagr. Thermochem. 3 (1979) 9–18.
[28] P. Flewitt, Reassessment of Monotectoid Loop (beta-Nb+beta-Zr) in Niobium-Zirconium System, J. Appl. Crystallogr. 5 (1972) 423-425.
[29] P. Van Effenterre, Rapport CEA-R-4390, CEA, Centre d'Etudes Nucléaires de Saclay, 1972.
[30] B.A. Rogers, D.F. Atkins, Zirconium-Columbium diagram, Trans AIME. 203 (1955) 1034-1041.
[31] A. Knapton, Niobium and Tantalum Alloys, J. -Common Met. 2 (1960) 113–124.
[32] C.E. Lundin, R.H. Cox, The determination of the equilibrium phase diagram Zirconium-Niobium, US Atomic Energy Commision, 1960.
[33] A. Dwight, Alloying behaviour of Columbium, Columbium Metall. 10 (1961) 383-406.
[34] H. Richter, P. Wincierz, K. Anderko, Constitution of Zirconium-Niobium alloys, J - Common Met. 4 (1962) 252.
[35] A.R. Miedema, P.F. de Châtel, F.R. de Boer, Cohesion in alloys — fundamentals of a semi-empirical model, Phys. BC. 100 (1980) 1–28.
[36] C. Colinet, A. Pasturel, P. Hicter, Trends in cohesive energy of transition metal alloys, Calphad-Comput. Coupling Phase Diagr. Thermochem. . 9 (1985) 71–99.
[37] Y. Kwon, J. Corbett, The Zirconium-Tin System, with Particular Attention to the Zr5Sn3-Zr5Sn4 Region and Zr4Sn, Chem. Mater. 2 (1990) 27–33.
[38] D. Mcpherson, M. Hansen, The System Zirconium-Tin, Trans. Am. Soc. Met. 45 (1953) 915–933.
[39] G.R. Speich, S. Kulin, Am Soc Met. (1953) 197–207.
[40] G. Gran, S. Andersson, The Crystal Structures of Zr5Sn3 and Zr3Sn, Acta Chem. Scand. 14 (1960) 956–957.
[41] G. Carpenter, E. Ibrahim, J. Watters, The Aging Response of Zirconium-Tin Alloys, J. Nucl. Mater. 102 (1981) 280–291.
[42] D. Arias, L. Roberti, The Solubility of Tin in Alpha-Zirconium and Beta-Zirconium Below 1000-Degrees-C, J. Nucl. Mater. 118 (1983) 143–149.
[43] N. Subasic, Thermodynamic evaluation of Sn-Zr phase diagram, Calphad-Comput. Coupling Phase Diagr. Thermochem. 22 (1998) 157–165.
[44] N. Dupin, I. Ansara, C. Servant, C. Toffolon, C. Lemaignan, J.C. Brachet, A thermodynamic database for zirconium alloys, J. Nucl. Mater. 275 (1999) 287–295.
[45] W.Y. Kim, T. Takasugi, Laves phase fields in Cr-Zr-Nb and Cr-Zr-Hf alloy systems, Scr. Mater. 48 (2003) 559–563.
[46] I. Kornilov, S.P. Alisova, P.B. Budberg, Equilibrium phase diagram for the NbCr2-ZrCr2 metallic compound system, Inorg Mater. 1 (1965) 1993–1995.
[47] W.-B. Wang, H.-J. Lu, J.-Y. Shen, X.-G. Lu, Y.-L. He, Experimental investigation of phase equilibria in the Zr-Nb-Cr system at 1573 K and 1373 K, J. Nucl. Mater. 465 (2015) 626–632.

[48] O.S. Ivanov, V.K. Grigorovich, Structure and properties of zirconium alloys, Int. Conf. Geneva Pap. Sov. Sci. Mosc. 3 (1959) 439.
[49] N.G. Soboleva, Y.M. Sokolovskaya, V. Agafonov, M.A. Fyedorova, Physicochemical investigation of the ternary system niobium-zirconium-tin, Strukt Faz Fazovye Prevrashch Diagrammy Sostoyaniya Met Sist. (1974) 149–152.
[50] N.V. Korotkova, PHASE EQUILIBRIA IN THE Zr-Nb-Sn SYSTEM, Izv. Akad. Nauk SSSR Met. 4 (1990) 202–208.
[51] J.-C. Crivello, R. Souques, A. Breidi, N. Bourgeois, J.-M. Joubert, ZenGen, a tool to generate ordered configurations for systematic first-principles calculations: The Cr–Mo–Ni–Re system as a case study, Calphad-Comput. Coupling Phase Diagr. Thermochem. . 51 (2015) 233–240.
[52] G. Kresse, J. Furthmüller, Efficient iterative schemes for ab initio total-energy calculations using a plane-wave basis set, Phys. Rev. B. 54 (1996) 11169–11186.
[53] G. Kresse, D. Joubert, From ultrasoft pseudopotentials to the projector augmented-wave method, Phys. Rev. B. 59 (1999) 1758–1775.
[54] J.P. Perdew, K. Burke, M. Ernzerhof, Generalized Gradient Approximation Made Simple, Phys. Rev. Lett. 77 (1996) 3865–3868.
[55] P. Blöchl, Projector augmented-wave method, Phys. Rev. B. 50 (1994) 17953.
[56] A. Zunger, S.-H. Wei, L.G. Ferreira, J.E. Bernard, Special quasirandom structures, Phys. Rev. Lett. 65 (1990) 353–356.
[57] C. Jiang, C. Wolverton, J. Sofo, L.-Q. Chen, Z.-K. Liu, First-principles study of binary bcc alloys using special quasirandom structures, Phys. Rev. B. 69 (2004) 214202.
[58] D. Shin, R. Arróyave, Z.-K. Liu, A. Van de Walle, Thermodynamic properties of binary hcp solution phases from special quasirandom structures, Phys. Rev. B. 74 (2006) 024204.
[59] M.G. Valishev, Izvest Akad Nauk SSS. 4 (1992) 46.
[60] V.S. Sudavtsova, Raspavy. 1 (1990) 88.

Figure caption:

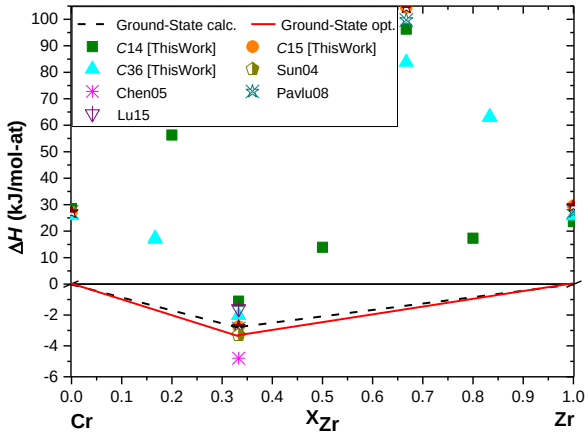

Figure 1: Calculated formation enthalpies of the Laves phase in the Cr–Zr system compared to data from literature.

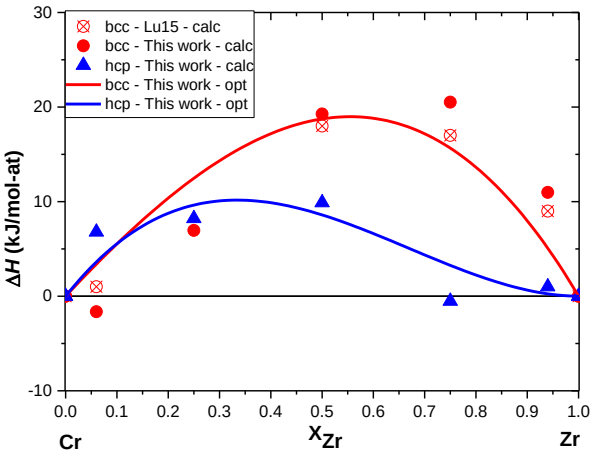

Figure 2: Calculated mixing enthalpies of the *A*2 and *A*3 solid solutions in the Cr–Zr system compared to data from literature

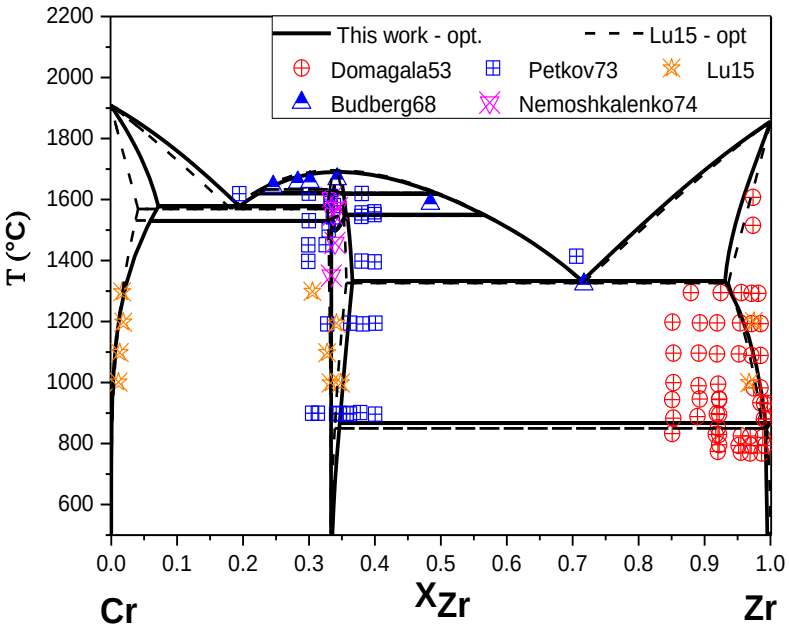

Figure 3: Calculated Cr–Zr system compared to experimental data.

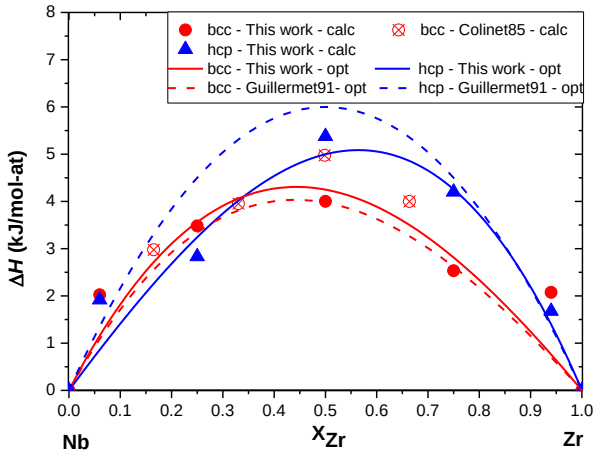

Figure 4: Calculated mixing enthalpies of the *A*2 and *A*3 solid solutions in the Nb–Zr system compared to data from literature.

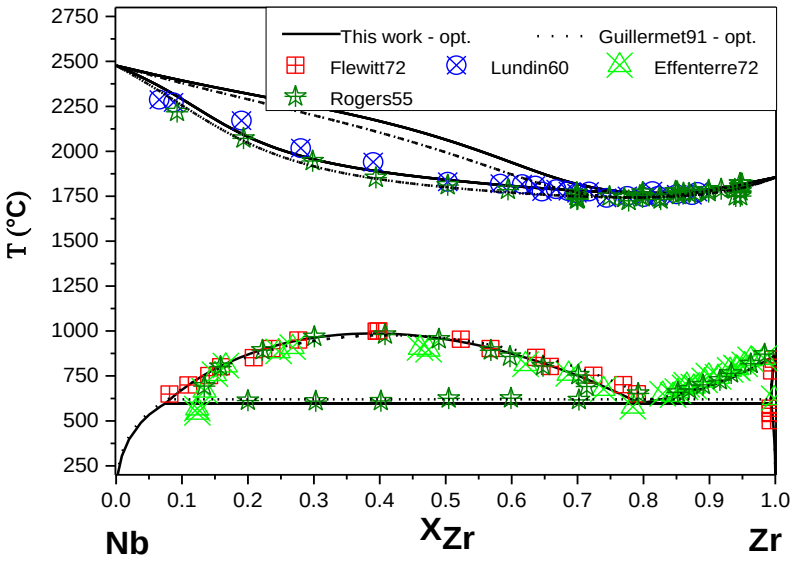

Figure 5: Calculated Nb–Zr system compared to experimental data

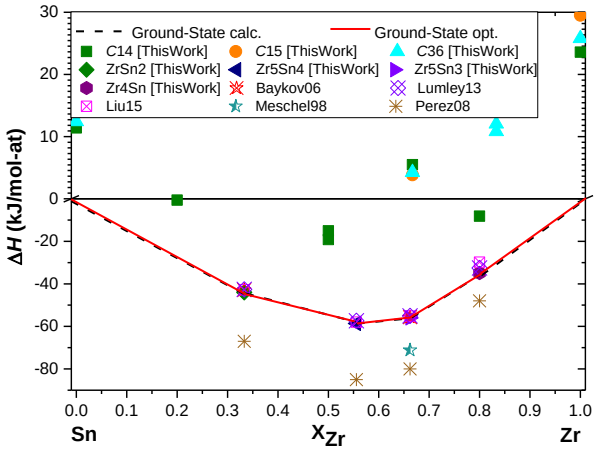

Figure 6: Calculated formation enthalpies of the *A*15, η and $ZrSn_2$ phases in the Sn–Zr system compared to data from literature.

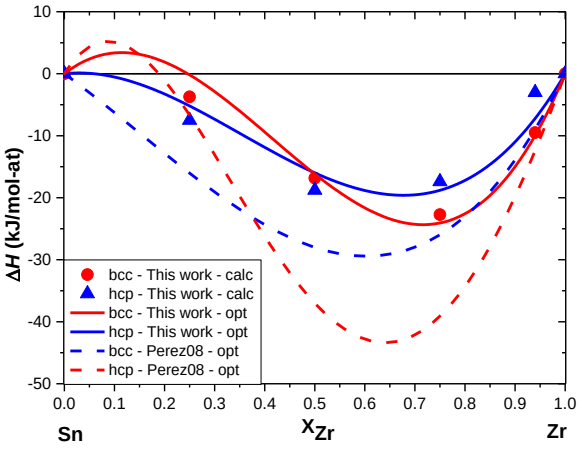

Figure 7: Calculated mixing enthalpies of the *A*2 and *A*3 solid solutions in the Sn–Zr system compared to data from literature

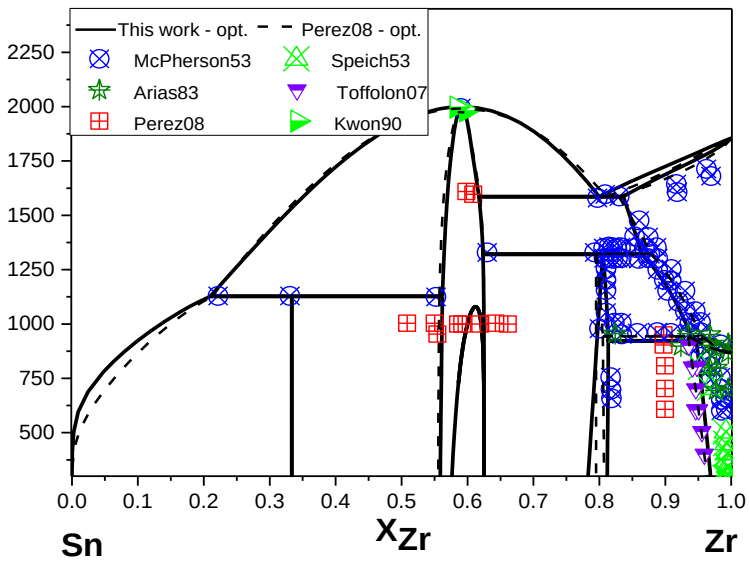

Figure 8: Calculated Sn–Zr system compared to experimental data

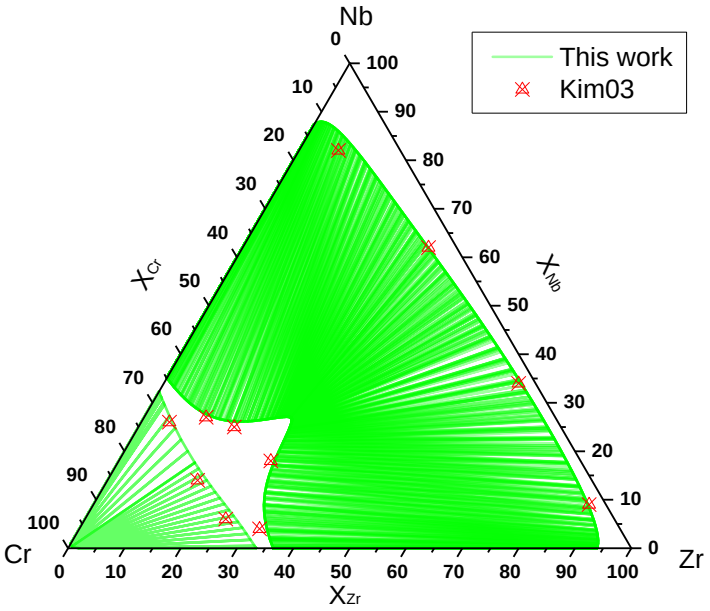

Figure 9: Calculated isothermal section at 1300 °C of the Cr–Nb–Zr system compared to experimental data

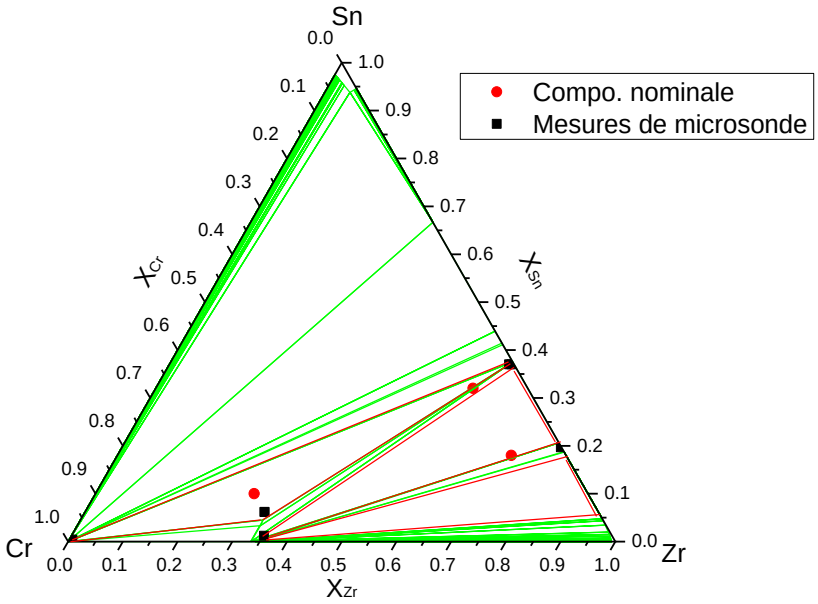

Figure 10: Calculated isothermal section at 900 °C of the Cr–Sn–Zr system compared to experimental data

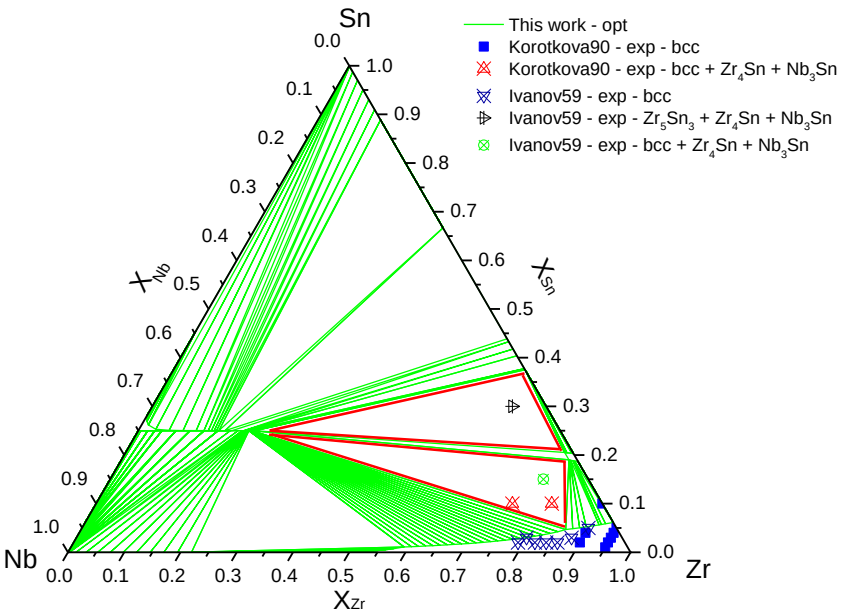

Figure 11: Calculated isothermal section at 950 °C of the Nb–Sn–Zr system compared to experimental data

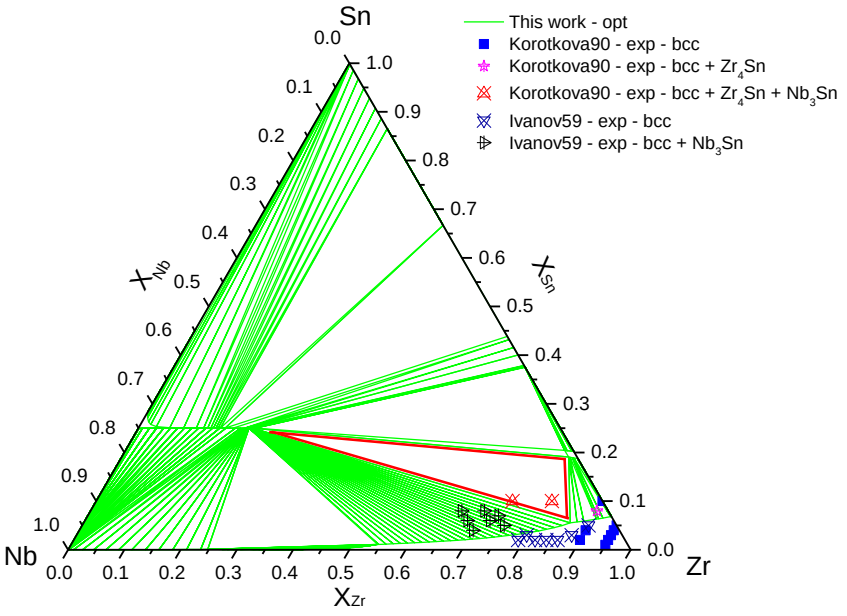

Figure 12: Calculated isothermal section at 1000 °C of the Nb–Sn–Zr system compared to experimental data

Table caption:

Table 1: Crystallographic description and sublattice model of the phases of the Cr–Nb–Sn–Zr system

Phase	Space group	Wyckoff position	Crystallographic site	Sublattice modelling
*C*14	*P6₃/mmc* (194)	2*a*; 4*f; 6h*	3	$(Cr,Nb,Sn,Zr)_4\,(Cr,Nb,Sn,Zr)_2\,(Cr,Nb,Sn,Zr)_6$
*C*15	*Fd*-3*m* (227)	8*a*; 16*d*	2	$(Cr,Nb,Sn,Zr)_2\,(Cr,Nb,Sn,Zr)_1$
*C*36	*P6₃/mmc* (194)	4*e*; 4*f;* 4*f;* 8*i; !*8*i*	3	$(Cr,Nb,Sn,Zr)_4\,(Cr,Nb,Sn,Zr)_4\,(Cr,Nb,Sn,Zr)_{16}$
η	*P6₃/mmc* (194)	*4d; 6g; 6g; 2b*	3	$(Zr)_5\,(Sn)_3\,(Sn,Va)_1$
$ZrSn_2$	*Fddd* (70)	16*f*; 16*g*; 16*g*	3	$(Zr)\,(Sn)_2$
*A*15	*Pm*-3*n* (223)	2*a*; 6*c*	2	$(Nb,Sn,Zr)_1\,(Nb,Sn,Zr)_3$

Table 2: Optimized thermodynamic parameters for the Cr–Zr system from the present work

Phase	Parameters (J/mol)
Liquid	${}^0L_{Cr,Zr} = -539.0 - 1.597*T$ ${}^1L_{Cr,Zr} = -155.6 - 0.7468*T$ ${}^2L_{Cr,Zr} = -828.5 - 0.9211*T$
*A*2	${}^0L_{Cr,Zr} = 75832 - 31.780*T$ ${}^1L_{Cr,Zr} = 17683 - 11.343*T$
*A*3	${}^0L_{Cr,Zr} = 34447 + 45*T$ ${}^1L_{Cr,Zr} = 34012 + 20.005*T$
*C*14 $(Cr, Zr)_4\,(Cr, Zr)_2\,(Cr, Zr)_6$	$G_{Cr:Cr:Cr} = 342291 + 12GHSERCR$ $G_{Cr:Zr:Cr} = 675355 + 10GHSERCR + 2GHSERZR$ $G_{Zr:Cr:Cr} = -20102 - 56.55*T + 8GHSERCR + 4GHSERZR$ $G_{Cr:Cr:Zr} = 809015 + 6GHSERCR + 6GHSERZR$ $G_{Zr:Zr:Cr} = 166978 + 6GHSERCR + 6GHSERZR$ $G_{Cr:Zr:Zr} = 1155553 + 4GHSERCR + 8GHSERZR$ $G_{Zr:Cr:Zr} = 207811 + 2GHSERCR + 10GHSERZR$ $G_{Zr:Zr:Zr} = 282926 + 12GHSERZR$ ${}^0L_{Cr,Zr:Cr:Cr} = 20004 + 10.045*T$ ${}^0L_{Zr:Cr:Cr,Zr} = -22500 - 8.929*T$
*C*15 $(Cr, Zr)_1\,(Cr, Zr)_2$	$G_{Cr:Cr} = 81518 + 3GHSERCR$ $G_{Zr:Cr} = -9973 - 11.422*T + 2GHSERCR + GHSERZR$ $G_{Cr:Zr} = 313559 + 2GHSERZR + GHSERCR$ $G_{Zr:Zr} = 88549 + 3GHSERZR$ ${}^0L_{Cr,Zr:Cr} = -8976$ ${}^0L_{Zr:Cr,Zr} = -15150$

*C*36 $(Cr, Zr)_4 (Cr, Zr)_4 (Cr, Zr)_{16}$	$G_{Cr:Cr:Cr}$ = 621157 + 24GHSERCR $G_{Zr:Cr:Cr}$ = 407179 + 20GHSERCR + 4GHSERZR $G_{Cr:Zr:Cr}$ = 417367 + 20GHSERCR + 4GHSERZR $G_{Zr:Zr:Cr}$ = – 62568-101.42*T + 16GHSERCR + 8GHSERZR $G_{Cr:Cr:Zr}$ = 2011613 + 8GHSERCR + 16GHSERZR $G_{Zr:Cr:Zr}$ = 1510437 + 4GHSERCR + 20GHSERZR $G_{Cr:Zr:Zr}$ = 1518505 + 4GHSERCR + 20GHSERZR $G_{Zr:Zr:Zr}$ = 618997 + 24GHSERZR

Table 3: Optimized thermodynamic parameters for the Nb–Zr system from the present work

Phase	**Parameters (J/mol)**
Liquid	${}^0L_{Nb,Zr}$ = 13192 ${}^1L_{Nb,Zr}$ = 10055
*A*2	${}^0L_{Nb,Zr}$ = +14390+4.26*T ${}^1L_{Nb,Zr}$ = 3417
*A*3	${}^0L_{Nb,Zr}$ = 24411

Table 4: Optimized thermodynamic parameters for the Sn–Zr system from the present work

Phase	**Parameters (J/mol)**
Liquide	${}^0L_{Sn,Zr}$ = – 102754 – 18.37*T ${}^1L_{Sn,Zr}$ = 21641
*A*2	${}^0L_{Sn,Zr}$ = – 62600 – 36.55*T ${}^1L_{Sn,Zr}$ = 120000 – 47*T
*A*3	${}^0L_{Sn,Zr}$ = – 75965 – 8.70*T ${}^1L_{Sn,Zr}$ = 90127 – 44.5*T ${}^2L_{Sn,Zr}$ = – 56618
*A*15 $(Nb,Sn,Zr)_1 (Nb,Sn,Zr)_3$	$G_{Sn:Sn}$ = 30031+19.45*T+4*GHSERSN $G_{Sn:Zr}$ = – 179972+26.53*T+GHSERSN+3*GHSERZR $G_{Zr:Sn}$ = 201296+3*GHSERSN+GHSERZR $G_{Zr:Zr}$ = 50012+4*GHSERZR ${}^0L_{Sn,Zr:Zr}$ = – 79990 ${}^1L_{Sn,Zr:Zr}$ = – 139990
η $(Zr)_5 (Sn)_3 (Sn,Va)_1$	$G_{Zr:Sn:Sn}$ = – 527796+1.0*T+4*GHSERSN+5*GHSERZR $G_{Zr:Sn:Va}$ = – 448112+3*GHSERSN+5*GHSERZR ${}^0L_{Zr:Sn:Sn,Va}$ = 9490 – 25*T ${}^1L_{Zr:Sn:Sn,Va}$ = – 72999+30*T
$ZrSn_2$	$G_{Zr:Sn}$ = – 131946+2.68*T+2*GHSERSN+GHSERZR

Table 5: Optimized thermodynamic parameters for the Cr–Nb–Zr system from the present work

Phase	Parameters (J/mol)
*A*2	${}^0L_{Cr,Nb,Zr} = -5000$ ${}^1L_{Cr,Nb,Zr} = -10200$ ${}^2L_{Cr,Nb,Zr} = 69500$
*C*14 $(Cr,Nb,Zr)_4$ $(Cr,Nb,Zr)_2(Cr,Nb,Zr)_6$	$G_{Cr:Nb:Zr}$= 753299+4*GHSERCR+2*GHSERNB+6*GHSERZR $G_{Zr:Nb:Cr}$ = 50676+6*GHSERCR+2*GHSERNB+4*GHSERZR $G_{Nb:Zr:Cr}$ = 232337+6*GHSERCR+4*GHSERNB+2*GHSERZR $G_{Nb:Cr:Zr}$= 335767+2*GHSERCR+4*GHSERNB+6*GHSERZR $G_{Zr:Cr:Nb}$ = 60678+2*GHSERCR+6*GHSERNB+4*GHSERZR $G_{Cr:Zr:Nb}$ = 986560+4*GHSERCR+6*GHSERNB+2*GHSERZR
*C*15 $(Cr,Nb,Zr)_2(Cr,Nb,Zr)_1$	${}^0L_{Cr:Zr,Cr,Nb} = -140650$ ${}^0L_{Cr:Nb,Zr} = -18000$
*C*36 $(Cr,Nb,Zr)_4$ $(Cr,Nb,Zr)_4(Cr,Nb,Zr)_{16}$	$G_{Cr:Zr:Nb}$ = 847500+4*GHSERCR+16*GHSERNB+4*GHSERZR $G_{Zr:Cr:Nb}$ = 829117+4*GHSERCR+16*GHSERNB+4*GHSERZR $G_{Zr:Nb:Cr}$ = −70241+16*GHSERCR+4*GHSERNB+4*GHSERZR $G_{Cr:Nb:Zr}$= 1756055+4*GHSERCR+4*GHSERNB+16*GHSERZR $G_{Nb:Zr:Cr}$ = −67632+16*GHSERCR+4*GHSERNB+4*GHSERZR $G_{Nb:Cr:Zr}$= 1734867+4*GHSERCR+4*GHSERNB+16*GHSERZR

Table 6: Composition and annealing treatments of the Cr–Sn–Zr samples prepared in this work

Composition	Annealing treatment	Structure (XRD)	Lattice parameters (Rietveld)	Composition (EPMA)
$Cr_{61}Sn_{10}Zr_{29}$	20 days at 900°C	*C*14 Zr_5Sn_3 bcc	*a*=5.192 Å; *c*=8.478 Å *a*=8.467 Å; *c*=5.789 Å *a*=2.892 Å	$Cr_{61}Sn_{6.2}Zr_{32.8}$ $Cr_{0.6}Sn_{36.5}Zr_{62.9}$ $Cr_{99}Sn_{0.4}Zr_{0.6}$
$Cr_{10}Sn_{34}Zr_{56}$	20 days at 900°C	*C*15 Zr_5Sn_3	*a*=7.243 Å *a*=8.507 Å; *c*=5.819 Å	$Cr_{64.3}Sn_{1.4}Zr_{34.3}$ $Cr_{0.9}Sn_{37}Zr_{62.1}$
$Cr_{10}Sn_{18}Zr_{72}$	20 days at 900°C	*C*15 *A*15 Zr_5Sn_3	*a*=7.211 Å *a*=5.627 Å *a*=8.460 Å; c=5.781 Å	$Cr_{63.6}Sn_{1.2}Zr_{35.2}$ $Cr_{0.1}Sn_{19.7}Zr_{80.2}$ $Cr_{0.4}Sn_{37.7}Zr_{61.9}$

Table 7: Optimized thermodynamic parameters for the Cr–Sn–Zr system from the present work

Phase	Parameter (J/mol)
*C*14 $(Cr,Sn,Zr)_4$ $(Cr,Sn,Zr)_2(Cr,Sn,Zr)_6$	$G_{Cr:Sn:Zr}$= 966809+4*GHSERCR+2*GHSERSN+6*GHSERZR $G_{Zr:Sn:Cr}$ = −192018 − 40*T+6*GHSERCR+2*GHSERSN+4*GHSERZR $G_{Sn:Zr:Cr}$ = 407848+6*GHSERCR+4*GHSERSN+2*GHSERZR $G_{Sn:Cr:Zr}$ = 132860+2*GHSERCR+4*GHSERSN+6*GHSERZR $G_{Zr:Cr:Sn}$ = −77206+2*GHSERCR+6*GHSERSN+4*GHSERZR $G_{Cr:Zr:Sn}$ = 531853+4*GHSERCR+6*GHSERSN+2*GHSERZR

	${}^{0}L_{Zr:Cr,Sn:Cr} = -105000$
*C*36 $(Cr,Sn,Zr)_4$ $(Cr,Sn,Zr)_4(Cr,Sn,Zr)_{16}$	$G_{Cr:Zr:Sn}$= 1048332+4*GHSERCR+16*GHSERSN+4*GHSERZR $G_{Zr:Cr:Sn}$= 1030802+4*GHSERCR+16*GHSERSN+4*GHSERZR $G_{Zr:Sn:Cr}$ = 149604+16*GHSERCR+4*GHSERSN+4*GHSERZR $G_{Cr:Sn:Zr}$= 1307473+4*GHSERCR+4*GHSERSN+16*GHSERZR $G_{Sn:Zr:Cr}$ = 148836+16*GHSERCR+4*GHSERSN+4*GHSERZR $G_{Sn:Cr:Zr}$= 889553+4*GHSERCR+4*GHSERSN+16*GHSERZR

Table 8: Optimized thermodynamic parameters for the Nb–Sn–Zr system from the present work

Phase	**Parameter (J/mol)**
*C*14 $(Nb,Sn,Zr)_4$ $(Nb,Sn,Zr)_2(Nb,Sn,Zr)_6$	$G_{Nb:Sn:Zr}$ = 232855+4*GHSERNB+2*GHSERSN+6*GHSERZR $G_{Zr:Sn:Nb}$ = – 171875+6*GHSERNB+2*GHSERSN+4*GHSERZR $G_{Sn:Zr:Nb}$ = 205489+6*GHSERNB+4*GHSERSN+2*GHSERZR $G_{Sn:Nb:Zr}$ = 70871+2*GHSERNB+4*GHSERSN+6*GHSERZR $G_{Zr:Nb:Sn}$ = – 138571+2*GHSERNB+6*GHSERSN+4*GHSERZR $G_{Nb:Zr:Sn}$ = 306588+4*GHSERNB+6*GHSERSN+2*GHSERZR
*A*15 $(Nb,Sn,Zr)_3(Nb,Sn,Zr)_1$	${}^{0}L_{Nb,Zr:Sn} = -125000$ ${}^{1}L_{Nb,Zr:Sn} = -472000 + 15*T$ ${}^{2}L_{Nb,Zr:Sn} = -410000$
*C*36 $(Nb,Sn,Zr)_4$ $(Nb,Sn,Zr)_4(Nb,Sn,Zr)_{16}$	$G_{Nb:Sn:Zr}$ = 966213+4*GHSERNB+2*GHSERSN+6*GHSERZR $G_{Zr:Sn:Nb}$ = 156838+6*GHSERNB+2*GHSERSN+4*GHSERZR $G_{Sn:Zr:Nb}$ = 121336+6*GHSERNB+4*GHSERSN+2*GHSERZR $G_{Sn:Nb:Zr}$ = 556700+2*GHSERNB+4*GHSERSN+6*GHSERZR $G_{Zr:Nb:Sn}$ = 910146+2*GHSERNB+6*GHSERSN+4*GHSERZR $G_{Nb:Zr:Sn}$ = 966213+4*GHSERNB+6*GHSERSN+2*GHSERZR